

SPEAR: Exact Gradient Inversion of Batches in Federated Learning

Dimitar I. Dimitrov¹ Maximilian Baader¹ Mark Niklas Müller¹ Martin Vechev¹

Abstract

Federated learning is a popular framework for collaborative machine learning where multiple clients only share gradient updates on their local data with the server and not the actual data. Unfortunately, it was recently shown that gradient inversion attacks can reconstruct this data from these shared gradients. Existing attacks enable exact reconstruction only for a batch size of $b = 1$ in the important honest-but-curious setting, with larger batches permitting only approximate reconstruction. In this work, we propose *the first algorithm reconstructing whole batches with $b > 1$ exactly*. This approach combines mathematical insights into the explicit low-rank structure of gradients with a sampling-based algorithm. Crucially, we leverage ReLU-induced gradient sparsity to precisely filter out large numbers of incorrect samples, making a final reconstruction step tractable. We provide an efficient GPU implementation for fully connected networks and show that it recovers batches of $b \lesssim 25$ elements exactly while being tractable for large network widths and depths.

1. Introduction

Federated learning has emerged as the dominant paradigm for training machine learning models collaboratively without sharing sensitive data (McMahan et al., 2017). Instead, a central server sends the current model to all clients which then compute gradients with their private data and send them back to the server. There, the gradients are aggregated and used to update the model. Using this approach sensitive data never leaves the clients’ machines, aligning it better with data privacy regulations such as the General Data Protection Regulation (GDPR) and California Consumer Privacy Act (CCPA).

¹Department of Computer Science, ETH Zurich, Zurich, Switzerland. Correspondence to: Dimitar I. Dimitrov <dimitadi@inf.ethz.ch>.

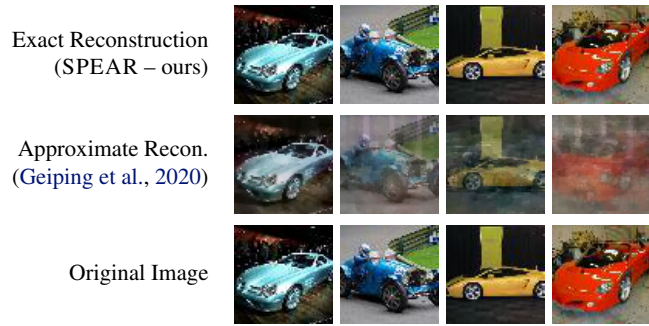


Figure 1. A sample of four images from a batch of $b = 20$, reconstructed using our SPEAR (top) or the prior state-of-the-art Geiping et al. (2020) (mid), compared to the ground truth (bottom).

Gradient Inversion Attacks Recent work has shown that an honest-but-curious server can use the shared gradient updates to reconstruct the sensitive client data (Zhu et al., 2019; Dimitrov et al., 2022). However, while *exact* reconstruction was shown to be possible for batch sizes of $b = 1$ (Phong et al., 2018; Zhu & Blaschko, 2021), it was assumed to be infeasible for larger batches. This led to a line of research on approximate methods that sacrificed reconstruction quality in order to recover batches of $b > 1$ inputs (Geng et al., 2021; Vero et al., 2022; Kariyappa et al., 2023). In this paper we challenge this fundamental assumption and, for the first time, show that exact reconstruction is possible for batch sizes $b > 1$.

This Work: Exact Reconstruction of Batches We propose the *first gradient inversion attack reconstructing inputs exactly for batch sizes $b > 1$* in the honest-but-curious setting. We illustrate the resulting reconstruction quality in Figure 1, comparing it to approximate reconstructions for a batch of $b = 20$ images (Geiping et al., 2020).

Our approach leverages two key properties of gradient updates in fully connected ReLU networks: First, these gradients have a specific *low-rank structure* due to small batch sizes $b \ll n, m$ compared to the input dimensionality n and the hidden dimension m . Second, the (unknown) gradients with respect to the inputs of the first ReLU layer are sparse due to the ReLU function itself. We now combine these properties with ideas from sparsely-used dictionary learning Spielman et al. (2012) to propose a sampling-based algorithm, called SPEAR (**S**parsity **E**xploiting **A**ctivation

Recovery) and show that it succeeds with high probability for $b < m$. While SPEAR scales exponentially with batch size b , we provide a highly parallelized GPU implementation of SPEAR, which empirically allows us to reconstruct batches of size up to $b \lesssim 25$ exactly even for large inputs (TINYIMAGENET) and networks (widths up to 2000 and depths up to 9) in around one minute.

Main Contributions:

- The first method to *exactly reconstruct* complete batches of size $b > 1$ in the honest-but-curious setting.
- SPEAR: an algorithm that leverages *low rankness* and ReLU-induced *sparsity of gradients* in a highly parallelizable sampling-based algorithm for exact gradient inversion that succeeds with high probability.
- A highly parallelized GPU implementation of SPEAR, which we empirically demonstrate to be effective across a wide range of settings.

2. Method Overview

We first introduce our setting before giving a high-level overview of our gradient inversion attack SPEAR. A depiction of SPEAR is provided in Figure 2.

Setting We consider a neural network f containing a linear layer $z = \mathbf{W}\mathbf{x} + \mathbf{b}$ followed by ReLU activations $\mathbf{y} = \text{ReLU}(z)$ trained with some loss function \mathcal{L} . Let now $\mathbf{X} \in \mathbb{R}^{n \times b}$ be a batch of b inputs to this linear layer $\mathbf{Z} = \mathbf{W}\mathbf{X} + (\mathbf{b} \dots | \mathbf{b})$, with weights $\mathbf{W} \in \mathbb{R}^{m \times n}$, bias $\mathbf{b} \in \mathbb{R}^m$ and output $\mathbf{Z} \in \mathbb{R}^{m \times b}$. Further, let $\mathbf{Y} \in \mathbb{R}^{m \times b}$ be the result of applying the ReLU activation to \mathbf{Z} , i.e., $\mathbf{Y} = \text{ReLU}(\mathbf{Z})$ and assume $b \leq m, n$.

The goal of gradient inversion now is to *recover the inputs* \mathbf{X} (up to permutation) given the gradients $\frac{\partial \mathcal{L}}{\partial \mathbf{W}}$ and $\frac{\partial \mathcal{L}}{\partial \mathbf{b}}$ (see Figure 2, i).

Low-Rank Decomposition We first show that the weight gradient $\frac{\partial \mathcal{L}}{\partial \mathbf{W}} = \frac{\partial \mathcal{L}}{\partial \mathbf{Z}} \mathbf{X}^\top$ naturally has a low rank $b \leq m, n$ (Theorem 3.1) and can therefore be decomposed as $\frac{\partial \mathcal{L}}{\partial \mathbf{W}} = \mathbf{L}\mathbf{R}$ into the two matrices $\mathbf{L} \in \mathbb{R}^{m \times b}$ and $\mathbf{R} \in \mathbb{R}^{b \times n}$ using SVD (Figure 2, ii). We then prove the existence disaggregation matrix $\mathbf{Q} = (\mathbf{q}_1 | \dots | \mathbf{q}_b) \in \text{GL}_b(\mathbb{R})$, allowing us to express the inputs $\mathbf{X}^\top = \mathbf{Q}^{-1}\mathbf{R}$ and activation gradients $\frac{\partial \mathcal{L}}{\partial \mathbf{Z}} = \mathbf{L}\mathbf{Q}$ (Theorem 3.2). Next, we leverage the sparsity of $\frac{\partial \mathcal{L}}{\partial \mathbf{Z}}$ to recover \mathbf{Q} exactly.

ReLU Induced Sparsity We show that ReLU layers induce sparse activation gradients $\frac{\partial \mathcal{L}}{\partial \mathbf{Z}}$ (§3.2). We then leverage this sparsity to show that, with high probability, there exist submatrices $\mathbf{L}_A \in \mathbb{R}^{b-1 \times b}$ of \mathbf{L} , such that their kernel is an unscaled column $\bar{\mathbf{q}}_i$ of our disaggregation matrix

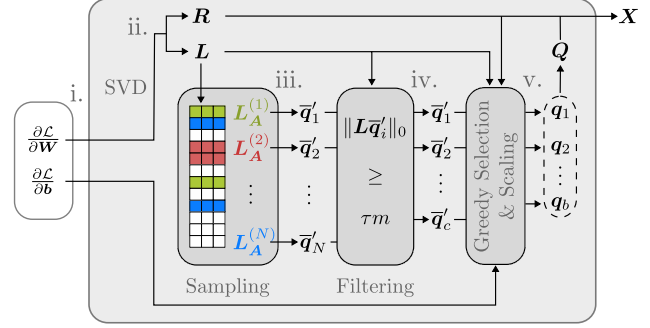


Figure 2. Overview of SPEAR. The gradient $\frac{\partial \mathcal{L}}{\partial \mathbf{W}}$ is decomposed to \mathbf{R} and \mathbf{L} . Sampling gives us N proposal directions, which get filtered down to c candidates via a sparsity criterion filtering all proposals that fail to pass the sparsity threshold τm . A greedy selection method selects b ($b = \text{batchsize}$) directions. Scale recovery via $\frac{\partial \mathcal{L}}{\partial \mathbf{b}}$ returns the disaggregation matrix \mathbf{Q} and thus the inputs \mathbf{X} .

\mathbf{Q} , i.e., $\ker(\mathbf{L}_A) = \text{span}(\mathbf{q}_i)$, for all $i \in \{1, \dots, b\}$ (Theorem 3.4). Given these unscaled columns $\bar{\mathbf{q}}_i$, we recover their scale by leveraging the bias gradient $\frac{\partial \mathcal{L}}{\partial \mathbf{b}}$ (Theorem 3.6).

Sampling and Filtering Directions To identify the submatrices \mathbf{L}_A of \mathbf{L} which induce these directions $\bar{\mathbf{q}}_i$, we propose a sampling-based approach (§4.1): We randomly sample $b - 1$ rows of \mathbf{L} to obtain an \mathbf{L}_A and thus proposal direction $\bar{\mathbf{q}}'_i = \ker(\mathbf{L}_A)$ (Figure 2 iii). Crucially, the product $\mathbf{L}\bar{\mathbf{q}}'_i = \frac{\partial \mathcal{L}}{\partial \mathbf{z}_i}$ will recover a column of the sparse activation gradient $\frac{\partial \mathcal{L}}{\partial \mathbf{Z}}$ for correct directions $\bar{\mathbf{q}}'_i$ while incorrect directions will recover a dense linear combination of such columns. This sparsity difference allows us to filter a large number N of proposal directions obtained for different submatrices \mathbf{L}_A until $c \gtrsim b$ unique candidates remain (Figure 2 iv).

Greedy Direction Selection We now have to select the correct b directions from our set of c candidates (Figure 2, v). To this end, we build an initial solution \mathbf{Q}' from the b directions inducing the highest sparsity in $\frac{\partial \mathcal{L}}{\partial \mathbf{Z}} = \mathbf{L}\mathbf{Q}'$. To assess the quality of this solution \mathbf{Q}' , we introduce the sparsity matching score σ which measures how well the sparsity of the activation gradients $\frac{\partial \mathcal{L}}{\partial \mathbf{Z}}$ matches the ReLU activation pattern induced by the reconstructed input $\mathbf{X}'^\top = \mathbf{Q}'^{-1}\mathbf{R}$. Finally, we greedily optimize \mathbf{Q}' to maximize the sparsity matching score, by iteratively replacing an element \mathbf{q}'_i of \mathbf{Q}' with the candidate direction \mathbf{q}'_j yielding the greatest improvement in σ until convergence. We can then validate the resulting input $\mathbf{X}^\top = \mathbf{Q}^{-1}\mathbf{R}$ by checking whether it induces the correct gradients.

Algorithm We formalize this as Algorithm 1 in §5 and show that it succeeds with high probability for $b < m$.

3. Gradient Inversion via Sparsity and Low-Rankness

In this Section, we will demonstrate that both low rankness and sparsity arise naturally for gradients of fully connected ReLU networks and explain theoretically how we recover \mathbf{X} . Specifically, in §3.1, we first argue that $\frac{\partial \mathcal{L}}{\partial \mathbf{W}} = \frac{\partial \mathcal{L}}{\partial \mathbf{Z}} \mathbf{X}^T$ follows directly from the chain rule. We then show that for every decomposition $\frac{\partial \mathcal{L}}{\partial \mathbf{W}} = \mathbf{L}\mathbf{R}$, there exists an unknown disaggregation matrix \mathbf{Q} allowing us to reconstruct $\mathbf{X}^T = \mathbf{Q}^{-1}\mathbf{R}$ and $\frac{\partial \mathcal{L}}{\partial \mathbf{Z}} = \mathbf{L}\mathbf{Q}$. The remainder of our approach then focuses on recovering \mathbf{Q} . To this end, we show in §3.2 that ReLU layers induce sparsity in $\frac{\partial \mathcal{L}}{\partial \mathbf{Z}}$, which we then leveraged in §3.3 to reconstruct the columns of \mathbf{Q} up to scale. Finally, in §3.4, we show how the scale of \mathbf{Q} 's columns can be recovered from $\frac{\partial \mathcal{L}}{\partial \mathbf{b}}$. Unless otherwise noted, we defer all proofs to App. A.

3.1. Explicit Low-Rank Representation of $\frac{\partial \mathcal{L}}{\partial \mathbf{W}}$

We first show that the weight gradients $\frac{\partial \mathcal{L}}{\partial \mathbf{W}}$ can be written as follows:

Theorem 3.1. *The network's gradient w.r.t. the weights \mathbf{W} can be represented as the matrix product:*

$$\frac{\partial \mathcal{L}}{\partial \mathbf{W}} = \frac{\partial \mathcal{L}}{\partial \mathbf{Z}} \mathbf{X}^T. \quad (1)$$

For batch sizes $b \leq n, m$, the dimensionalities of $\frac{\partial \mathcal{L}}{\partial \mathbf{Z}} \in \mathbb{R}^{m \times b}$ and $\mathbf{X} \in \mathbb{R}^{n \times b}$ in Equation (1) directly yield that the rank of $\frac{\partial \mathcal{L}}{\partial \mathbf{W}}$ is at most b . This confirms the observations of Kariyappa et al. (2023) and shows that \mathbf{X} and $\frac{\partial \mathcal{L}}{\partial \mathbf{Z}}$ correspond to a specific low-rank decomposition of $\frac{\partial \mathcal{L}}{\partial \mathbf{W}}$.

To actually find this decomposition and thus recover \mathbf{X} , we first consider an arbitrary decomposition of the form $\frac{\partial \mathcal{L}}{\partial \mathbf{W}} = \mathbf{L}\mathbf{R}$, where $\mathbf{L} \in \mathbb{R}^{m \times b}$ and $\mathbf{R} \in \mathbb{R}^{b \times n}$ are of maximal rank. We chose the decomposition obtained via the reduced SVD decomposition of $\frac{\partial \mathcal{L}}{\partial \mathbf{W}} = \mathbf{U}\mathbf{S}\mathbf{V}$ by setting $\mathbf{L} = \mathbf{U}\mathbf{S}^{\frac{1}{2}}$ and $\mathbf{R} = \mathbf{S}^{\frac{1}{2}}\mathbf{V}$, where $\mathbf{U} \in \mathbb{R}^{m \times b}$, $\mathbf{S} \in \mathbb{R}^{b \times b}$ and $\mathbf{V} \in \mathbb{R}^{b \times n}$.

We now show that there exists a unique disaggregation matrix \mathbf{Q} recovering \mathbf{X} and $\frac{\partial \mathcal{L}}{\partial \mathbf{Z}}$ from \mathbf{L} and \mathbf{R} :

Theorem 3.2. *If the gradient $\frac{\partial \mathcal{L}}{\partial \mathbf{Z}}$ and the input matrix \mathbf{X} are of full-rank and $b \leq n, m$, then there exists a unique matrix $\mathbf{Q} \in \mathbb{R}^{b \times b}$ of full-rank s.t.:*

$$\frac{\partial \mathcal{L}}{\partial \mathbf{Z}} = \mathbf{L}\mathbf{Q}, \quad \text{and} \quad (2)$$

$$\mathbf{X}^T = \mathbf{Q}^{-1}\mathbf{R}. \quad (3)$$

This is a direct consequence of the following lemma:

Lemma 3.3. *Let $b, n, m \in \mathbb{N}$ such that $b < n, m$. Further, let $\mathbf{A}, \mathbf{L} \in \mathbb{R}^{m \times b}$ and $\mathbf{B}, \mathbf{R} \in \mathbb{R}^{b \times n}$ be matrices of*

maximal rank, satisfying $\mathbf{AB} = \mathbf{LR}$. Then there exists a unique disaggregation matrix $\mathbf{Q} \in GL_b(\mathbb{R})$ s.t. $\mathbf{A} = \mathbf{L}\mathbf{Q}$, and $\mathbf{B} = \mathbf{Q}^{-1}\mathbf{R}$.

Intuitively, Theorem 3.2 states that under most circumstances, reconstructing the input matrix \mathbf{X} and the gradient matrix $\frac{\partial \mathcal{L}}{\partial \mathbf{Z}}$ is equivalent to recovering the unique disaggregation matrix \mathbf{Q} . We will continue to show how the ReLU-induced sparsity patterns in $\frac{\partial \mathcal{L}}{\partial \mathbf{Z}}$ or \mathbf{X} can be leveraged to recover \mathbf{Q} exactly.

3.2. ReLU-Induced Sparsity

ReLU activation layers can induce sparsity both in the gradient $\frac{\partial \mathcal{L}}{\partial \mathbf{Z}}$ (if the ReLU activation succeeds the considered linear layer) or in the input (if the ReLU activation precedes the considered linear layer).

Gradient Sparsity If a ReLU activation succeeds the linear layer, i.e., $\mathbf{Y} = \text{ReLU}(\mathbf{Z})$, we have:

$$\frac{\partial \mathcal{L}}{\partial \mathbf{Z}} = \frac{\partial \mathcal{L}}{\partial \mathbf{Y}} \odot \mathbb{1}_{[\mathbf{Z} > 0]}, \quad (4)$$

where \odot is the elementwise multiplication and $\mathbb{1}_{[\mathbf{Z} > 0]}$ is a matrix of 0s and 1s with each entry indicating if the corresponding entry in \mathbf{Z} is positive. At initialization, roughly half of the entries in \mathbf{Z} are positive, making $\frac{\partial \mathcal{L}}{\partial \mathbf{Z}}$ sparse with roughly half the entries being 0.

Input Sparsity ReLU activations also introduce sparsity if the linear layer in question is preceded by a ReLU activation layer. In this case, $\mathbf{X} = \text{ReLU}(\tilde{\mathbf{Z}})$ will be sparse with roughly half of its entries being 0s at initialization.

Note that for all but the first and the last layer of a fully connected network, we have sparsity in both, \mathbf{X} and $\frac{\partial \mathcal{L}}{\partial \mathbf{Z}}$. Due to the symmetry of Equations (2) and (3), our method can be applied in all three arising sparsity settings. In the remainder of this work, we assume w.l.o.g. that only $\frac{\partial \mathcal{L}}{\partial \mathbf{Z}}$ is sparse, corresponding to the first layer of a fully connected network. We now describe how to leverage this sparsity to compute the disaggregation matrix \mathbf{Q} and thus recover the input batch \mathbf{X} .

3.3. Breaking Aggregation through Sparsity

Our exact recovery algorithm for the disaggregation matrix \mathbf{Q} is based on the following insight:

If we can construct two submatrices $\mathbf{A} \in \mathbb{R}^{b-1 \times b}$ and $\mathbf{L}_A \in \mathbb{R}^{b-1 \times b}$ by choosing $b-1$ rows with the same indices from $\frac{\partial \mathcal{L}}{\partial \mathbf{Z}}$ and \mathbf{L} , respectively, such that \mathbf{A} has full rank and an all-zero i^{th} column, then the kernel $\ker(\mathbf{L}_A)$ of \mathbf{L}_A contains a column \mathbf{q}_i of \mathbf{Q} up to scale. We formalize this as follows:

Theorem 3.4. *Let $\frac{\partial \mathcal{L}}{\partial \mathbf{Z}}$ and \mathbf{X} be of full rank and $\mathbf{A} \in \mathbb{R}^{b-1 \times b}$ a submatrix of $\frac{\partial \mathcal{L}}{\partial \mathbf{Z}}$ of full rank such that the i^{th}*

column is $\mathbf{0}$ for some $i \in \{1, \dots, b\}$. Further let \mathbf{Q} be as in Theorem 3.2. Then, there exists a full-rank submatrix $\mathbf{L}_A \in \mathbb{R}^{b-1 \times b}$ of \mathbf{L} such that $\text{span}(\mathbf{q}_i) = \ker(\mathbf{L}_A)$ for the i^{th} column \mathbf{q}_i of $\mathbf{Q} = (\mathbf{q}_1 | \dots | \mathbf{q}_b)$.

Proof. Pick an $i \in \{1, \dots, b\}$. By assumption, there exists a submatrix $\mathbf{A} \in \mathbb{R}^{b-1 \times b}$ of $\frac{\partial \mathcal{L}}{\partial \mathbf{Z}}$ of rank $b - 1$ such that the i^{th} column is $\mathbf{0}$. Now, we construct \mathbf{L}_A by taking the rows from \mathbf{L} with the same indices as the rows of \mathbf{A} have in $\frac{\partial \mathcal{L}}{\partial \mathbf{Z}}$.

As $\frac{\partial \mathcal{L}}{\partial \mathbf{Z}}$ and \mathbf{X} have full rank, by Theorem 3.2, we know that $\frac{\partial \mathcal{L}}{\partial \mathbf{Z}} = \mathbf{L}\mathbf{Q}$, and hence $\mathbf{A} = \mathbf{L}_A\mathbf{Q}$. Multiplying from the right with \mathbf{e}_i yields

$$\mathbf{0} = \mathbf{A}\mathbf{e}_i = \mathbf{L}_A\mathbf{Q}\mathbf{e}_i = \mathbf{L}_A\mathbf{q}_i,$$

and hence $\ker(\mathbf{L}_A) \supseteq \text{span}(\mathbf{q}_i)$. Further, as $\text{rank}(\mathbf{A}) = b - 1$ and $\text{rank}(\mathbf{Q}) = b$, we have that $\text{rank}(\mathbf{L}_A) = b - 1$. With the rank-nullity theorem we see that $\dim(\ker(\mathbf{L}_A)) = 1$ and hence $\ker(\mathbf{L}_A) = \text{span}(\mathbf{q}_i)$. \square

As $\frac{\partial \mathcal{L}}{\partial \mathbf{Z}}$ is not known a priori, we can not simply search for such a set of rows. Instead, we have to sample submatrices \mathbf{L}_A of \mathbf{L} at random and then filter them using the approach discussed in §4. However, we will show in §5.2 that we will find suitable submatrices with high probability for $b < m$ due to the sparsity of $\frac{\partial \mathcal{L}}{\partial \mathbf{Z}}$ and the large number $\binom{m}{b-1}$ of possible submatrices.

We will now discuss how to recover the scale of the columns \mathbf{q}_i given their unscaled directions $\bar{\mathbf{q}}_i$ forming $\bar{\mathbf{Q}}$.

3.4. Obtaining \mathbf{Q} : Recovering the Scale of columns in $\bar{\mathbf{Q}}$

Given a set of b correct directions $\bar{\mathbf{Q}} = (\bar{\mathbf{q}}_1 | \dots | \bar{\mathbf{q}}_b)$, we can recover their scale, enabling us to reconstruct \mathbf{X} , as follows.

We first represent the correctly scaled columns as $\mathbf{q}_i = c_i \cdot \bar{\mathbf{q}}_i$ with the unknown scale parameters $c_i \in \mathbb{R}$. Now, recovering the scale is equivalent to computing all c_i . To this end, we leverage the gradient w.r.t. the bias $\frac{\partial \mathcal{L}}{\partial \mathbf{b}}$:

Lemma 3.5. *The gradient w.r.t. the bias \mathbf{b} can be written in the form:*

$$\frac{\partial \mathcal{L}}{\partial \mathbf{b}} = \frac{\partial \mathcal{L}}{\partial \mathbf{Z}} \begin{bmatrix} 1 \\ \vdots \\ 1 \end{bmatrix}. \quad (5)$$

Thus, the coefficients c_i can be calculated as:

Theorem 3.6. *For any left inverse \mathbf{L}^{-L} of \mathbf{L} , we have:*

$$\begin{bmatrix} c_1 \\ \vdots \\ c_b \end{bmatrix} = \bar{\mathbf{Q}}^{-1} \mathbf{L}^{-L} \frac{\partial \mathcal{L}}{\partial \mathbf{b}} \quad (6)$$

Once we have computed the unscaled $\bar{\mathbf{Q}}$, we can directly obtain the disaggregation matrix $\mathbf{Q} = \bar{\mathbf{Q}} \text{diag}(c_1, \dots, c_b)$ allowing us to reconstruct the input $\mathbf{X}^\top = \mathbf{Q}^{-1} \mathbf{R}$. We now discuss how to sample and filter candidate directions $\bar{\mathbf{q}}_i$ to recover $\bar{\mathbf{Q}}$.

4. Efficient Filtering and Validation of Candidates

In the previous section, we saw that given the correct selection of submatrices \mathbf{L}_A , we can recover \mathbf{Q} directly. However, we do not know how to pick \mathbf{L}_A a priori. To solve this problem, we rely on a sampling-based approach: We first randomly sample submatrices \mathbf{L}_A of \mathbf{L} and corresponding direction candidates $\bar{\mathbf{q}}'$ spanning $\ker(\mathbf{L}_A)$. However, checking whether $\bar{\mathbf{q}}'$ is a valid direction is not straightforward as we do not know $\frac{\partial \mathcal{L}}{\partial \mathbf{Z}}$ and hence can not observe \mathbf{A} directly as reconstructing $\frac{\partial \mathcal{L}}{\partial \mathbf{Z}} = \mathbf{L}\mathbf{Q}$ requires the full \mathbf{Q} .

To address this, we propose a method to filter the majority of wrong proposals $\bar{\mathbf{q}}'$ using deduplication and a sparsity-based criterion (discussed in §4.1). This leaves us with a set of candidate directions $\mathcal{C} = \{\bar{\mathbf{q}}'_j\}_{j \in \{1, \dots, c\}}$, among which we then select the correct directions by greedily optimizing a novel sparsity matching score (discussed in §4.2).

4.1. Efficient Filtering of Directions $\bar{\mathbf{q}}'$

Filtering Mixtures via Sparsity It is highly likely ($p = (1 - \frac{1}{2^{b-1}})^b$) that a random submatrix of \mathbf{L} will not correspond to an \mathbf{A} with any $\mathbf{0}$ column. We filter these directions by leveraging the following insight. The kernel of such submatrices is spanned by a linear combination $\bar{\mathbf{q}}' = \sum_i \alpha_i \bar{\mathbf{q}}_i$. Thus $\mathbf{L}\bar{\mathbf{q}}'$ will be a linear combination of sparse columns of $\frac{\partial \mathcal{L}}{\partial \mathbf{Z}}$. As this sparsity structure is random, linear combinations will have much lower sparsity with high probability. We thus discard all candidates $\bar{\mathbf{q}}'$ with sparsity of $\mathbf{L}\bar{\mathbf{q}}'$ below a threshold τ , chosen to make the probability of falsely rejecting a correct direction $p_{f_r}(\tau, m) = \frac{1}{2^m} \sum_{i=0}^{\lfloor m \cdot \tau \rfloor} \binom{m}{i}$, obtained from the cumulative distribution function of the binomial distribution, small. For example for $m = 400$ and $p_{f_r}(\tau, m) < 10^{-5}$, we have $\tau = 0.395$. We obtain the candidate pool $\mathcal{C} = \{\bar{\mathbf{q}}'_j\}_{j \in \{1, \dots, c\}}$ from all samples that were not filtered this way.

Filtering Duplicates As it is highly likely to have multiple full-rank submatrices \mathbf{A} , whose i^{th} column is $\mathbf{0}$, we expect to sample the same proposal $\bar{\mathbf{q}}'_i$ multiple times. We remove these duplicates substantially reduces our search space.

4.2. Greedy Optimization

While filtering duplicates and linear combinations significantly reduces the number c of candidates, we usually still have to select a subset of $b < c$. Thus, we have $\binom{c}{b}$ possible b sized subsets, each inducing a candidate \mathbf{Q}' and thus \mathbf{X}' . A naive approach would be to compute the gradients for all \mathbf{X}' and compare them against the ground truth. However, this is computationally intractable even for moderate candidate numbers c .

To address this, we propose a greedy two-stage procedure

optimizing a novel sparsity matching score σ , solely relying on $\frac{\partial \mathcal{L}'}{\partial \mathbf{Z}}$ and \mathbf{Z}' . As both can be computed directly via \mathbf{Q}' , the procedure is local, does not need to backpropagate gradients and resolves the computational complexity issue mentioned at the beginning of this subsection while also accurately selecting the correct batch elements. Next, we explain the first stage.

Dictionary Learning (Spielman et al., 2012) As a first stage, we leverage a component of the algorithm proposed by Spielman et al. (2012) for sparsely-used dictionary learning. This approach is based on the insight that the subset of column vectors $\{\bar{\mathbf{q}}'_i\}_{i=1}^b$, yielding the sparsest full-rank gradient matrix $\frac{\partial \mathcal{L}}{\partial \mathbf{Z}}$ via Equation (2) is often correct. As the scaling of $\bar{\mathbf{q}}'_i$ does not change the sparsity in Equation (2), we can construct this subset \mathcal{B} by greedily collecting the b directions $\bar{\mathbf{q}}'_i$ with the highest corresponding sparsity that still increases the rank of \mathcal{B} . While this approach typically recovers most directions $\bar{\mathbf{q}}'_i$, it often misses directions whose gradients $\frac{\partial \mathcal{L}}{\partial \mathbf{z}_i}$ are less sparse by chance.

Sparsity Matching We alleviate this issue by introducing a second stage to the algorithm where we greedily optimize a novel correctness measure based solely on the gradients of the linear layer, which we call the sparsity matching coefficient σ .

Definition 4.1. Let σ_- be the number of non-positive entries in \mathbf{Z} whose corresponding entries in $\frac{\partial \mathcal{L}}{\partial \mathbf{Z}}$ are 0. Similarly, let σ_+ be the number of positive entries in \mathbf{Z} whose corresponding entries in $\frac{\partial \mathcal{L}}{\partial \mathbf{Z}}$ are not 0. We call their normalized sum the *sparsity matching coefficient* σ :

$$\sigma = \frac{\sigma_- + \sigma_+}{m \cdot b}.$$

Intuitively, this describes how well the pre-activation values \mathbf{Z} match the sparsity pattern of the gradients $\frac{\partial \mathcal{L}}{\partial \mathbf{Z}}$, induced by the succeeding ReLU layer $\mathbf{Y} = \text{ReLU}(\mathbf{Z})$, as shown in Equation (4).

While this sparsity matching coefficient σ can take values between 0 and 1, it is exactly $\sigma = 1$ for the correct \mathbf{X} , if the gradient $\frac{\partial \mathcal{L}}{\partial \mathbf{Y}}$ w.r.t. the ReLU output is dense, which is usually the case. We note that σ can be computed efficiently for arbitrary full rank matrix $\bar{\mathbf{Q}}'$ by computing $\frac{\partial \mathcal{L}'}{\partial \mathbf{Z}'} = \mathbf{L}\mathbf{Q}'$ and $\mathbf{Z}' = \mathbf{W}\mathbf{X}' + (\mathbf{b} | \dots | \mathbf{b})$ for $\mathbf{X}'^\top = \mathbf{Q}'^{-1}\mathbf{R}$.

To optimize σ , we initialize $\bar{\mathbf{Q}}'$ with the result of the greedy algorithm in Spielman et al. (2012), and then greedily swap the pair of vectors $\bar{\mathbf{q}}'_i$ that improves σ the most, while not changing the rank, until convergence.

5. Final Algorithm and Complexity Analysis

In this section, we first present our final algorithm SPEAR (§5.1) and then analyse its expected complexity and failure probability (§5.2).

Algorithm 1 SPEAR

```

1: INPUT:  $m, n, \mathbf{W}, \mathbf{b}, \frac{\partial \mathcal{L}}{\partial \mathbf{W}}, \frac{\partial \mathcal{L}}{\partial \mathbf{b}}$ 
2:  $\mathbf{L}, \mathbf{R}, b \leftarrow \text{LOWRANKDECOMPOSE}(\frac{\partial \mathcal{L}}{\partial \mathbf{W}})$ 
3: for  $i = 1$  to  $N$  do
4:   Sample a submatrix  $\mathbf{L}_A \in \mathbb{R}^{b-1 \times b}$  of  $\mathbf{L}$ 
5:    $\bar{\mathbf{q}}'_i \leftarrow \text{ker}(\mathbf{L}_A)$ 
6:   if  $\text{sparsity}(\mathbf{L}\bar{\mathbf{q}}'_i) \geq \tau * m$  and  $\bar{\mathbf{q}}'_i \notin \mathcal{C}$  then
7:      $\mathcal{C} \leftarrow \mathcal{C} \cup \{\bar{\mathbf{q}}'_i\}$ 
8:      $\sigma, \mathbf{X}' \leftarrow \text{GREEDYFILTER}(\mathbf{L}, \mathbf{R}, \mathbf{W}, \mathbf{b}, \frac{\partial \mathcal{L}}{\partial \mathbf{b}}, \mathcal{C})$ 
9:     if  $\sigma = 1$  then
10:       return  $\mathbf{X}'$ 
11:  $\sigma, \mathbf{X}' \leftarrow \text{GREEDYFILTER}(\mathcal{C})$ 
12: return  $\mathbf{X}'$ 

```

5.1. Final Algorithm

We formalize our gradient inversion attack SPEAR in Algorithm 1 and outline it below. First, we compute the low-rank decomposition $\frac{\partial \mathcal{L}}{\partial \mathbf{W}} = \mathbf{L}\mathbf{R}$ of the weight gradient $\frac{\partial \mathcal{L}}{\partial \mathbf{W}}$ via reduced SVD, allowing us to recover the batch size b as the rank of $\frac{\partial \mathcal{L}}{\partial \mathbf{W}}$ (Line 2). We now sample (at most N) submatrices \mathbf{L}_A of \mathbf{L} and compute proposal directions $\bar{\mathbf{q}}'_i$ as their kernel $\text{ker}(\mathbf{L}_A)$ via SVD (Lines 4 and 5). We note that our implementation parallelizes both sampling and SVD computation (Lines 4 and 5) on a GPU. We then filter the proposal directions $\bar{\mathbf{q}}'_i$ based on their sparsity (Line 6), adding them to our candidate pool \mathcal{C} if they haven't been recovered already and are sufficiently sparse (Line 7). Once our candidate pool contains at least b directions, we begin constructing candidate input reconstructions \mathbf{X}' using our two-stage greedy algorithm GREEDYFILTER (Line 8), discussed in §4.2. If this reconstruction leads to a solution with sparsity matching coefficient $\sigma = 1$, we terminate early and return the corresponding candidate solution (Line 9). Otherwise, we continue sampling until we have reached N samples and return the best reconstruction we can obtain from the resulting candidate pool (Line 11). The pseudocode for COMPUTESIGMA (Algorithm 2) and GREEDYFILTER (Algorithm 3) are deferred to App. B.

5.2. Analysis

In this section, we will analyze SPEAR w.r.t. the number of submatrices we *expect* to sample until we have recovered all b correct directions $\bar{\mathbf{q}}'_i$ (Lemma 5.2), and the probability of failing to recover all b correct directions despite checking all possible submatrices of \mathbf{L} (Lemma 5.3). For an analysis of the number of submatrices we have to sample until we have recovered all b correct directions $\bar{\mathbf{q}}'_i$ *with high probability*, we point to Lemma A.1. Further, as before, we defer all proofs also to App. A.

Expected Number of Required Samples To determine the expected number of required samples until we have

recovered the correct b direction vectors \bar{q}_i , we first compute a lower bound on the probability q of sampling a submatrix which satisfies the conditions of Theorem 3.4 for an arbitrary column i in \bar{Q} and then use the coupon collector problem to compute the expected number of required samples.

We can lower bound the probability of a submatrix $A \in \mathbb{R}^{b-1 \times b}$, randomly sampled as $b-1$ rows of $\frac{\partial \mathcal{L}}{\partial \mathbf{Z}}$, having exactly one all-zero column and being full rank as follows:

Lemma 5.1. *Let $A \in \mathbb{R}^{b-1 \times b}$ be submatrix of the gradient $\frac{\partial \mathcal{L}}{\partial \mathbf{Z}}$ obtained by sampling $b-1$ rows uniformly at random without replacement, where each element of $\frac{\partial \mathcal{L}}{\partial \mathbf{Z}}$ is distributed i.i.d. as $\frac{\partial \mathcal{L}}{\partial \mathbf{Z}_{j,k}} = \zeta |\epsilon|$ with $\epsilon \sim \mathcal{N}(\mu = 0, \sigma^2 > 0)$ and $\zeta \sim \text{Bernoulli}(p = \frac{1}{2})$. We then have the probability q of A having exactly one all-zero column and being full rank lower bounded by:*

$$\begin{aligned} q &\geq \frac{b}{2^{b-1}} \left(1 - \left(\frac{1}{2} + o_{b-1}(1)\right)^{b-1}\right) \\ &\geq \frac{b}{2^{b-1}} (1 - 0.939^{b-1}). \end{aligned}$$

We can now compute the expected number of submatrices n_{total}^* we have to draw until we have recovered all b correct direction vectors using the Coupon Collector Problem:

Lemma 5.2. *Assuming i.i.d. submatrices A following the distribution outlined in Lemma 5.1 and using Algorithm 1, we have the expected number of submatrices n_{total}^* required to recover all b correct direction vectors as:*

$$n_{\text{total}}^* = \frac{1}{q} \sum_{k=0}^{b-1} \frac{b}{b-k} = \frac{bH_b}{q} \approx \frac{1}{q} (b \log(b) + \gamma b + \frac{1}{2}),$$

where H_b is the b^{th} harmonic number and $\gamma \approx 0.57722$ the Euler-Mascheroni constant.

We validate this result experimentally in Figure 4 where we observe excellent agreement for wide networks ($m \gg b$) and obtain, e.g., $n_{\text{total}}^* \approx 1.8 \times 10^5$ for a batch size of $b = 16$.

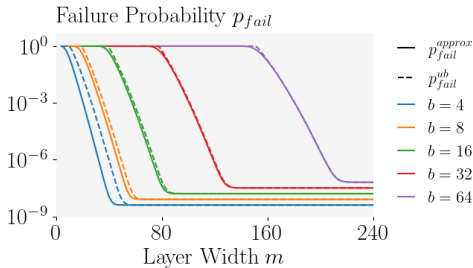


Figure 3. Visualizations of the upper bound ($p_{\text{fail}}^{\text{ub}}$, dashed) on and approximation of ($p_{\text{fail}}^{\text{approx}}$, solid) the failure probability of SPEAR for different batch sizes b and network widths m for $p_{fr} = 10^{-9}$.

Failure Probability We now analyze the probability of SPEAR failing despite considering all possible submatrices of L and obtain:

Lemma 5.3. *Under the same assumptions as in Lemma 5.1, we have an upper bound on the failure probability $p_{\text{fail}}^{\text{ub}}$ of Algorithm 1 even when sampling exhaustively as:*

$$\begin{aligned} p_{\text{fail}}^{\text{ub}} &\leq b \left(1 - \sum_{k=b-1}^m \binom{m}{k} \frac{1}{2^m} \left(1 - 0.939^{(b-1)\binom{k}{b-1}}\right)\right) \\ &\quad + 1 - (1 - p_{fr})^b, \end{aligned}$$

where p_{fr} is the probability of a correct direction vector being falsely rejected by our sparsity filter (§4.1).

If we assume the full-rankness of submatrices A to i) occur with probability $1 - (\frac{1}{2} - o_{b-1}(1))^{b-1}$ for $o_{b-1}(1) \approx 0$ (true for large b (Tikhomirov, 2020)) and ii) be independent between submatrices, we instead obtain:

$$\begin{aligned} p_{\text{fail}}^{\text{approx}} &\approx 1 - \left(\sum_{k=b-1}^m \binom{m}{k} \frac{1}{2^m} \left(1 - 0.5^{(b-1)\binom{k}{b-1}}\right)\right)^b \\ &\quad + 1 - (1 - p_{fr})^b. \end{aligned}$$

We illustrate this bound in Figure 3 and empirically validate this bound in Figure 8 and observe the true failure probability to lie between $p_{\text{fail}}^{\text{approx}}$ and $p_{\text{fail}}^{\text{ub}}$.

6. Empirical Evaluation

In this section, we empirically evaluate the effectiveness of SPEAR on MNIST (LeCun et al., 2010), CIFAR-10 (Krizhevsky et al., 2009), and TINYIMAGENET (Le & Yang, 2015) across a wide range of settings. In addition to the reconstruction quality metrics PSNR, SSIM, MSE, and LPIPS, commonly used to evaluate gradient inversion attacks, we report accuracy as the portion of batches for which we recovered all batch elements exactly (up to numerical errors) and the number of sampled submatrices (number of iterations).

Experimental Setup For all reported experiments, we use our highly parallelized PyTorch-based (Paszke et al., 2019) GPU implementation of SPEAR. Unless indicated otherwise, we run all of our experiments with a batch size of $b = 20$ CIFAR-10 images using a 6 layer fully-connected ReLU network with a width of $m = 200$ and choose τ to achieve a false rejection rate of $p_{fr} \leq 10^{-5}$.

6.1. Main Results

We evaluate SPEAR on MNIST, CIFAR-10, and TINYIMAGENET, reporting results in Table 1. Across datasets, SPEAR can reconstruct almost all batches perfectly, achieving PSNRs of 100 and above even at a batch size of $b = 20$. As these results indicate a significantly better reconstruction than any other method applicable to batch sizes $b > 1$, we omit a detailed quantitative comparison to prior work.

Table 1. Mean reconstruction quality metrics across 100 batches.

Dataset	PSNR \uparrow	SSIM \uparrow	MSE \downarrow	LPIPS \downarrow	Acc. \uparrow
MNIST	99.1	0.99998	2.61×10^{-6}	NaN	99%
CIFAR-10	106.6	0.99988	1.29×10^{-6}	1.16×10^{-5}	99%
TINYIMGNET	110.7	0.99971	27.05×10^{-6}	16.28×10^{-5}	99%

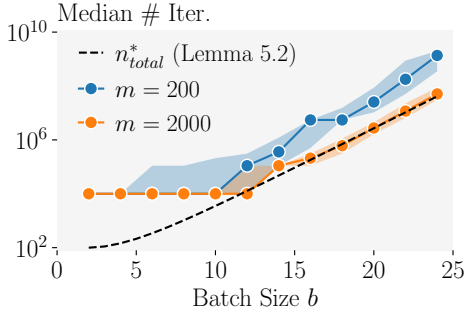


Figure 4. Effect of batch size b on the number of required submatrices. Expectation from Lemma 5.2 dashed and median (10^{th} to 90^{th} percentile shaded) depending on network width m solid. We always evaluate 10^4 submatrices in parallel, explaining the plateau.

6.2. Ablation Studies

Effect of Batch Size b We evaluate the effect of batch size b on accuracy and the required number of iterations n^*_{total} for a wide ($m = 2000$) and narrow ($m = 200$) network. While n^*_{total} increases exponentially with b , for both networks, the narrower network requires about 20 times more iterations than the wider network (see Figure 4). While trends for the wider network ($m \gg b$) are perfectly described by our theoretical results in §5.2, some independence assumptions are violated for the narrower network, explaining the larger number of required iterations. While we can recover all batches perfectly for the wider network, we see a sharp drop in accuracy from 99% at $b = 20$ to 63% at $b = 24$ (see Figure 6) for the narrower network. This is due to increasingly more batches requiring more than the $N = 2 \times 10^9$ submatrices we sample at most.

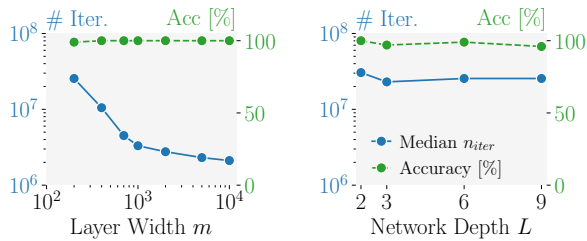


Figure 5. Accuracy (green) and number of median iterations (blue) for different network widths m at $L = 6$ (left) and depths L at $m = 200$ (right).

Effect of Network Architecture We visualize the performance of SPEAR across different network widths and depths in Figure 5. We observe that while accuracy is independent of both (given sufficient width $m \gg b$), the number of required iterations reduces with increasing width m .

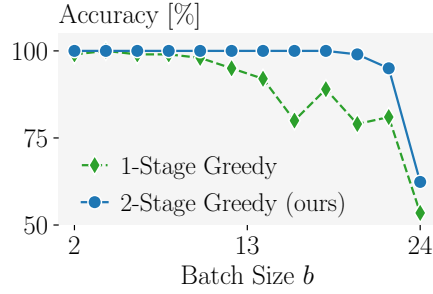


Figure 6. Effect of the second stage of our reconstruction algorithm discussed in §4.2, depending on the batch size b .

Effectiveness of our 2-Stage Greedy Algorithm We compare reconstruction success rate (accuracy) with and without the second stage of our greedy algorithm discussed in §4.2 in Figure 6. We observe that this second stage becomes increasingly important for larger batch size b .

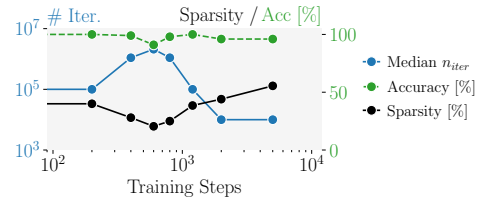


Figure 7. Effect of training (on MNIST) on the effectiveness of SPEAR at a batch size of $b = 10$ evaluated on training set.

Effect of Network Training We train a network on MNIST and evaluate SPEAR periodically during training, visualizing results in Figure 7. We observe that generally SPEAR performs very well on trained networks, with the number of required steps as on untrained networks. However, if the minimum column sparsity of $\frac{\partial \mathcal{L}}{\partial \mathbf{Z}}$ drops significantly as is the case for the checkpoints after 2000 and 3000 steps in the illustrated run performance drops slightly.

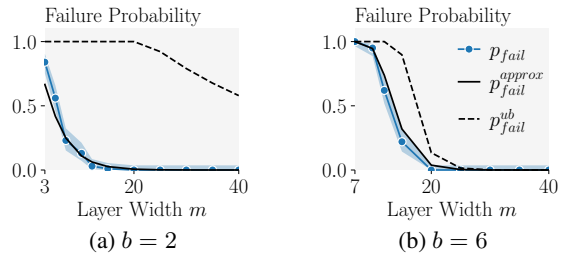


Figure 8. Empirical failure probability (blue) with 95% Clopper-Pearson confidence bounds (shaded blue) compared to the analytical upper bound (dashed line) and approximation (solid line) of the failure probability for different batch sizes b .

Failure Probabilities We validate our theoretical results on SPEAR’s failure rate (Lemma 5.3) in Figure 8. As this requires exhaustive sampling of all $\binom{m}{b-1}$ submatrices of \mathbf{L} we only consider small batch sizes $b \leq 10$ and networks $m \leq 40$. We observe that the empirical failure probability

(blue) with 95% Clopper-Pearson confidence bounds lies between the analytical upper bound (dashed line) and approximation (solid line). We conclude that in most settings, the number of required samples rather than complete failure is the limiting factor for SPEAR’s performance.

7. Related Work

In this section, we discuss how we relate to prior work.

Gradient Inversion Attacks Since gradient inversion attacks have been introduced (Zhu et al., 2019), two settings have emerged: In the *malicious setting*, the server does not adhere to the training protocol and can adversarially engineer network weights that maximize leaked information (Boenisch et al., 2021; Fowl et al., 2022b;a; Wen et al., 2022). In the strictly harder *honest-but-curious setting*, the server follows the training protocol but still aims to reconstruct client data. We target the honest-but-curious setting, where prior work has either recovered the input exactly for batch sizes of $b = 1$ (Phong et al., 2018; Zhu & Blaschko, 2021), or approximately for $b > 1$ (Geiping et al., 2020; Yin et al., 2021; Geng et al., 2021; Vero et al., 2022; Kariyappa et al., 2023). In this setting, we are the *first to reconstruct inputs exactly for batch sizes $b > 1$* .

Most closely related to our work is Kariyappa et al. (2023) which leverage the low-rank structure of the gradients to frame gradient inversion as a blind source separation problem, improving their approximate reconstructions. In contrast, we derive an *explicit* low-rank representation and additionally leverage gradient sparsity reconstruct inputs exactly.

Unlike a long line of prior work, we rely neither on any priors on the data distribution (Vero et al., 2022; Balunović et al., 2022a; Gupta et al., 2022; Li et al., 2022) nor on a reconstructed classification label (Geiping et al., 2020; Zhao et al., 2020; Geng et al., 2021; Yin et al., 2021; Vero et al., 2022). This allows our approach to be employed in a much wider range of settings where neither is available.

Defenses Against Gradient Inversion Defenses based on Differential Privacy (Abadi et al., 2016) add noise to the computed gradients on the client side, providing provable privacy guarantees at the cost of significantly reduced utility. Another line of work increases the empirical difficulty of inversion by increasing the effective batch size, by securely aggregating gradients from multiple clients (Bonawitz et al., 2016) or doing multiple gradient update steps locally before sharing an aggregated weight update (Dimitrov et al., 2022). Finally, different heuristic defenses such as gradient pruning (Zhu et al., 2019) have been proposed, although their effectiveness has been questioned (Balunović et al., 2022b).

Sparsely used Dictionary learning Recovering the disaggregation matrix Q is related to the well-studied problem of

sparsely-used dictionary learning. However, there the aim is to find the sparsest coefficient matrix (corresponding to our $\frac{\partial \mathcal{L}}{\partial \mathbf{Z}}$) and dense dictionary (Q^{-1}) encoding a given signal (\mathbf{L}) up to some error. In contrast, we do not search for the sparsest solution yielding an approximate reconstruction but a solution that exactly induces consistent \mathbf{X} and $\frac{\partial \mathcal{L}}{\partial \mathbf{Z}}$, which happens to be sparse.

Generally, sparsely-used dictionary learning is known to be NP-hard (Tillmann, 2014) and typically solved approximately (Aharon et al., 2006; Spielman et al., 2012; Sun et al., 2016). However, in specific cases, it can be solved exactly in polynomial time (Spielman et al., 2012). While $\frac{\partial \mathcal{L}}{\partial \mathbf{Z}}$ is not sufficiently sparse to satisfy these conditions, we draw inspiration from Spielman et al. (2012) in §4.

8. Limitations

In line with results showing that recovering the order of batch elements is generally impossible for gradient inversion (Geiping et al., 2020; Yin et al., 2021; Geng et al., 2021; Dimitrov et al., 2022), our approach only recovers the input \mathbf{X} up to permutation.

Further, we focus on recovering the inputs to fully connected layers such as they occur at the beginning of fully connected networks or as aggregation layers of many other architectures. Extending our approach to other layers is an interesting direction for future work. Similarly, we focus on FedSGD and believe that work on FedAvg is another interesting direction for future work.

Finally, our approach scales exponentially with batch size b . While it is practically effective for moderate batch sizes $b \lesssim 25$ and can be parallelized to a large degree, much larger batch sizes remain out of reach.

9. Conclusion

We propose SPEAR, the first algorithm permitting batches of $b > 1$ elements to be recovered exactly in the honest-but-curious setting. We show theoretically and empirically that SPEAR succeeds with high probability and experimentally demonstrates that our highly parallelized GPU implementation is effective across a wide range of settings, including batches of up to 24 elements and large networks and inputs.

We thereby demonstrate that contrary to prior belief, an exact reconstruction of batches is possible in the honest-but-curious setting, suggesting that federated learning on ReLU networks might be inherently more susceptible than previously thought. To still protect client privacy, large effective batch sizes, obtained, e.g., via secure aggregation across a large number of clients, might prove instrumental by making reconstruction computationally intractable.

10. Broader Impact

In this work, we demonstrate that contrary to prior belief, an exact reconstruction of batches is possible in the honest-but-curious setting for federated learning. As our work demonstrates the susceptibility of federated learning systems using ReLU networks, this work inevitably advances the capabilities of an adversary. Nonetheless, we believe this to be an important step in accurately assessing the risks and utilities of federated learning systems.

To still protect client privacy, large effective batch sizes, obtained, e.g., via secure aggregation across a large number of clients, might prove instrumental by making reconstruction computationally intractable. As gradient information and network states can be stored practically indefinitely, our work highlights the importance of proactively protecting client privacy in federated learning not only against current but future attacks. This underlines the importance of related work on provable privacy guarantees obtained via differential privacy.

References

- Abadi, M., Chu, A., Goodfellow, I. J., McMahan, H. B., Mironov, I., Talwar, K., and Zhang, L. Deep learning with differential privacy. In *CCS*, 2016.
- Aharon, M., Elad, M., and Bruckstein, A. K-svd: An algorithm for designing overcomplete dictionaries for sparse representation. *IEEE Transactions on signal processing*, 54(11):4311–4322, 2006.
- Balunović, M., Dimitrov, D. I., Jovanović, N., and Vechev, M. T. LAMP: extracting text from gradients with language model priors. In *NeurIPS*, 2022a.
- Balunović, M., Dimitrov, D. I., Staab, R., and Vechev, M. T. Bayesian framework for gradient leakage. In *ICLR*, 2022b.
- Boenisch, F., Dziedzic, A., Schuster, R., Shamsabadi, A. S., Shumailov, I., and Papernot, N. When the curious abandon honesty: Federated learning is not private. *arXiv*, 2021.
- Bonawitz, K. A., Ivanov, V., Kreuter, B., Marcedone, A., McMahan, H. B., Patel, S., Ramage, D., Segal, A., and Seth, K. Practical secure aggregation for federated learning on user-held data. *NIPS*, 2016.
- Chen, Z. *H2 Maths Handbook*. Educational Publishing House, 2011.
- Dimitrov, D. I., Balunović, M., Konstantinov, N., and Vechev, M. Data leakage in federated averaging. *Transactions on Machine Learning Research*, 2022. ISSN 2835-8856. URL <https://openreview.net/forum?id=e7A0B99zJf>.
- Fowl, L., Geiping, J., Reich, S., Wen, Y., Czaja, W., Goldblum, M., and Goldstein, T. Decepticons: Corrupted transformers breach privacy in federated learning for language models. *ICLR*, 2022a.
- Fowl, L. H., Geiping, J., Czaja, W., Goldblum, M., and Goldstein, T. Robbing the fed: Directly obtaining private data in federated learning with modified models. In *ICLR*, 2022b.
- Geiping, J., Bauermeister, H., Dröge, H., and Moeller, M. Inverting gradients-how easy is it to break privacy in federated learning? *NeurIPS*, 2020.
- Geng, J., Mou, Y., Li, F., Li, Q., Beyan, O., Decker, S., and Rong, C. Towards general deep leakage in federated learning. *arXiv*, 2021.
- Gupta, S., Huang, Y., Zhong, Z., Gao, T., Li, K., and Chen, D. Recovering private text in federated learning of language models. *Advances in Neural Information Processing Systems*, 35:8130–8143, 2022.
- Kariyappa, S., Guo, C., Maeng, K., Xiong, W., Suh, G. E., Qureshi, M. K., and Lee, H.-H. S. Cocktail party attack: Breaking aggregation-based privacy in federated learning using independent component analysis. In *International Conference on Machine Learning*, pp. 15884–15899. PMLR, 2023.
- Krizhevsky, A., Hinton, G., et al. Learning multiple layers of features from tiny images. 2009.
- Le, Y. and Yang, X. S. Tiny imagenet visual recognition challenge. *CS 231N*, 7(7), 2015.
- LeCun, Y., Cortes, C., and Burges, C. Mnist handwritten digit database. *ATT Labs [Online]*. Available: <http://yann.lecun.com/exdb/mnist>, 2, 2010.
- Li, Z., Zhang, J., Liu, L., and Liu, J. Auditing privacy defenses in federated learning via generative gradient leakage. In *Proceedings of the IEEE/CVF Conference on Computer Vision and Pattern Recognition*, pp. 10132–10142, 2022.
- McMahan, B., Moore, E., Ramage, D., Hampson, S., and y Arcas, B. A. Communication-efficient learning of deep networks from decentralized data. In *AISTATS*, 2017.
- Parameswaran, R. Statistics for experimenters: an introduction to design, data analysis, and model building. *JMR, Journal of Marketing Research (pre-1986)*, 16(000002): 291, 1979.
- Paszke, A., Gross, S., Massa, F., Lerer, A., Bradbury, J., Chanan, G., Killeen, T., Lin, Z., Gimelshein, N., Antiga, L., Desmaison, A., Köpf, A., Yang, E. Z., DeVito, Z., Raison, M., Tejani, A., Chilamkurthy, S., Steiner, B., Fang, L., Bai, J., and Chintala, S. Pytorch: An imperative style, high-performance deep learning library. In Wallach, H. M., Larochelle, H., Beygelzimer, A., d’Alché-Buc, F., Fox, E. B., and Garnett, R. (eds.), *Advances in Neural Information Processing Systems 32: Annual Conference on Neural Information Processing Systems 2019, NeurIPS 2019, December 8-14, 2019, Vancouver, BC, Canada*, pp. 8024–8035, 2019. URL <https://proceedings.neurips.cc/paper/2019/hash/bdbca288fee7f92f2bfa9f7012727740-Abstract.html>.
- Phong, L. T., Aono, Y., Hayashi, T., Wang, L., and Moriai, S. Privacy-preserving deep learning via additively homomorphic encryption. *IEEE Trans. Inf. Forensics Secur.*, (5), 2018.
- Spielman, D. A., Wang, H., and Wright, J. Exact recovery of sparsely-used dictionaries. In *Conference on Learning Theory*, pp. 37–1. JMLR Workshop and Conference Proceedings, 2012.

- Sun, J., Qu, Q., and Wright, J. Complete dictionary recovery over the sphere i: Overview and the geometric picture. *IEEE Transactions on Information Theory*, 63(2):853–884, 2016.
- Tao, T. and Vu, V. On random pm 1 matrices: singularity and determinant. In *Proceedings of the thirty-seventh annual ACM symposium on Theory of computing*, pp. 431–440, 2005.
- Tikhomirov, K. Singularity of random bernoulli matrices. *Annals of Mathematics*, 191(2):593–634, 2020.
- Tillmann, A. M. On the computational intractability of exact and approximate dictionary learning. *IEEE Signal Processing Letters*, 22(1):45–49, 2014.
- Vero, M., Balunović, M., Dimitrov, D. I., and Vechev, M. T. Data leakage in tabular federated learning. *ICML, 2022*.
- Wen, Y., Geiping, J., Fowl, L., Goldblum, M., and Goldstein, T. Fishing for user data in large-batch federated learning via gradient magnification. In *ICML, 2022*.
- Yin, H., Mallya, A., Vahdat, A., Alvarez, J. M., Kautz, J., and Molchanov, P. See through gradients: Image batch recovery via gradinversion. In *CVPR, 2021*.
- Zhao, B., Mopuri, K. R., and Bilen, H. idlg: Improved deep leakage from gradients. *arXiv*, 2020.
- Zhu, J. and Blaschko, M. B. R-GAP: recursive gradient attack on privacy. In *ICLR, 2021*.
- Zhu, L., Liu, Z., and Han, S. Deep leakage from gradients. In *NeurIPS, 2019*.

A. Deferred Proofs

Theorem 3.1. *The network's gradient w.r.t. the weights \mathbf{W} can be represented as the matrix product:*

$$\frac{\partial \mathcal{L}}{\partial \mathbf{W}} = \frac{\partial \mathcal{L}}{\partial \mathbf{Z}} \mathbf{X}^T. \quad (1)$$

Proof. We will use Einstein notation for this proof:

$$\begin{aligned} \frac{\partial \mathcal{L}}{\partial \mathbf{W}_i^j} &= \frac{\partial \mathcal{L}}{\partial \mathbf{Z}_k^l} \frac{\partial \mathbf{Z}_k^l}{\partial \mathbf{W}_i^j} \\ &= \frac{\partial \mathcal{L}}{\partial \mathbf{Z}_k^l} \frac{\partial (\mathbf{W}_k^m \mathbf{X}_m^l + b_k \delta^l)}{\partial \mathbf{W}_i^j} \\ &= \frac{\partial \mathcal{L}}{\partial \mathbf{Z}_k^l} \frac{\partial \mathbf{W}_k^m \mathbf{X}_m^l}{\partial \mathbf{W}_i^j} \\ &= \frac{\partial \mathcal{L}}{\partial \mathbf{Z}_k^l} \frac{\partial \mathbf{W}_k^m}{\partial \mathbf{W}_i^j} \mathbf{X}_m^l \\ &= \frac{\partial \mathcal{L}}{\partial \mathbf{Z}_k^l} \delta_k^i \delta_j^m \mathbf{X}_m^l \\ &= \frac{\partial \mathcal{L}}{\partial \mathbf{Z}_i^l} \mathbf{X}_j^l \\ &= \frac{\partial \mathcal{L}}{\partial \mathbf{Z}_i^l} (\mathbf{X}^T)^l_j. \end{aligned}$$

We note that δ_k^i is the Kronecker delta, that is $\delta_k^i = 1$ if $k = i$ and 0 otherwise. Further, $\delta^l = 1$ for all l . Hence we arrive at Equation (1). \square

Lemma 3.3. *Let $b, n, m \in \mathbb{N}$ such that $b < n, m$. Further, let $\mathbf{A}, \mathbf{L} \in \mathbb{R}^{m \times b}$ and $\mathbf{B}, \mathbf{R} \in \mathbb{R}^{b \times n}$ be matrices of maximal rank, satisfying $\mathbf{A}\mathbf{B} = \mathbf{L}\mathbf{R}$. Then there exists a unique disaggregation matrix $\mathbf{Q} \in GL_b(\mathbb{R})$ s.t. $\mathbf{A} = \mathbf{L}\mathbf{Q}$, and $\mathbf{B} = \mathbf{Q}^{-1}\mathbf{R}$.*

Proof. As $b \leq n, m$ and the matrices $\mathbf{A} \in \mathbb{R}^{m \times b}$ and $\mathbf{B} \in \mathbb{R}^{b \times n}$ have full rank, we know that there exists

- a left inverse $\mathbf{A}^{-L} \in \mathbb{R}^{b \times m}$ for \mathbf{A} : $\mathbf{A}^{-L}\mathbf{A} = \mathbf{I}_b$ and
- a right inverse $\mathbf{B}^{-R} \in \mathbb{R}^{n \times b}$ for \mathbf{B} : $\mathbf{B}\mathbf{B}^{-R} = \mathbf{I}_b$.

Thus, it follows from

$$\mathbf{A}^{-L}\mathbf{L}\mathbf{R}\mathbf{B}^{-R} = \mathbf{A}^{-L}\mathbf{A}\mathbf{B}\mathbf{B}^{-R} = \mathbf{I}_b,$$

that $(\mathbf{A}^{-L}\mathbf{L})^{-1} = \mathbf{R}\mathbf{B}^{-R}$. We now set $\mathbf{Q} = \mathbf{R}\mathbf{B}^{-R}$.

This \mathbf{Q} satisfies the required properties:

- $\mathbf{B} = \mathbf{Q}^{-1}\mathbf{R}$:

$$\mathbf{Q}^{-1}\mathbf{R} = \mathbf{A}^{-L}\mathbf{L}\mathbf{R} = \mathbf{A}^{-L}\mathbf{A}\mathbf{B} = \mathbf{B},$$

- $\mathbf{A} = \mathbf{L}\mathbf{Q}$:

$$\mathbf{L}\mathbf{Q} = \mathbf{L}\mathbf{R}\mathbf{B}^{-R} = \mathbf{A}\mathbf{B}\mathbf{B}^{-R} = \mathbf{A},$$

- Uniqueness: Assume we have \mathbf{Q}_1 and \mathbf{Q}_2 that satisfy $\mathbf{L}\mathbf{Q}_1 = \mathbf{L}\mathbf{Q}_2 = \mathbf{A}$. As \mathbf{L} is of rank b and $b \leq m$, there exists a left inverse \mathbf{L}^{-l} for \mathbf{L} : $\mathbf{L}^{-l}\mathbf{L} = \mathbf{I}_b$. Applying this left inverse to $\mathbf{L}\mathbf{Q}_1 = \mathbf{L}\mathbf{Q}_2$, directly yields $\mathbf{Q}_1 = \mathbf{Q}_2$, and hence we get uniqueness. \square

Lemma 3.5. *The gradient w.r.t. the bias \mathbf{b} can be written in the form:*

$$\frac{\partial \mathcal{L}}{\partial \mathbf{b}} = \frac{\partial \mathcal{L}}{\partial \mathbf{Z}} \begin{bmatrix} 1 \\ \vdots \\ 1 \end{bmatrix}. \quad (5)$$

Proof. We use again Einstein notation.

$$\begin{aligned} \frac{\partial \mathcal{L}}{\partial b_i} &= \frac{\partial \mathcal{L}}{\partial \mathbf{Z}_k^l} \frac{\partial \mathbf{Z}_k^l}{\partial b_i} \\ &= \frac{\partial \mathcal{L}}{\partial \mathbf{Z}_k^l} \frac{\partial (\mathbf{W}_k^m \mathbf{X}_m^l + \mathbf{b}_k \delta^l)}{\partial b_i} \\ &= \frac{\partial \mathcal{L}}{\partial \mathbf{Z}_k^l} \frac{\partial \mathbf{b}_k \delta^l}{\partial b_i} \\ &= \frac{\partial \mathcal{L}}{\partial \mathbf{Z}_k^l} \delta_k^i \delta^l \\ &= \frac{\partial \mathcal{L}}{\partial \mathbf{Z}_i^l} \delta^l. \end{aligned}$$

This concludes the proof. □

Theorem 3.6. *For any left inverse \mathbf{L}^{-L} of \mathbf{L} , we have:*

$$\begin{bmatrix} c_1 \\ \vdots \\ c_b \end{bmatrix} = \overline{\mathbf{Q}}^{-1} \mathbf{L}^{-L} \frac{\partial \mathcal{L}}{\partial \mathbf{b}} \quad (6)$$

Proof. The proof is straight forward. Using Lemma 3.5 and Theorem 3.2, we know that

$$\begin{aligned} \overline{\mathbf{Q}}^{-1} \mathbf{L}^{-L} \frac{\partial \mathcal{L}}{\partial \mathbf{b}} &= \overline{\mathbf{Q}}^{-1} \mathbf{L}^{-L} \frac{\partial \mathcal{L}}{\partial \mathbf{Z}} \begin{bmatrix} 1 \\ \vdots \\ 1 \end{bmatrix} \\ &= \overline{\mathbf{Q}}^{-1} \mathbf{L}^{-L} \mathbf{L} \mathbf{Q} \begin{bmatrix} 1 \\ \vdots \\ 1 \end{bmatrix} \\ &= \overline{\mathbf{Q}}^{-1} \mathbf{Q} \begin{bmatrix} 1 \\ \vdots \\ 1 \end{bmatrix} \\ &= \overline{\mathbf{Q}}^{-1} \overline{\mathbf{Q}} \text{diag}(c_1, \dots, c_b) \begin{bmatrix} 1 \\ \vdots \\ 1 \end{bmatrix} \\ &= \begin{bmatrix} c_1 \\ \vdots \\ c_b \end{bmatrix}. \end{aligned}$$

□

Lemma 5.1. *Let $\mathbf{A} \in \mathbb{R}^{b-1 \times b}$ be submatrix of the gradient $\frac{\partial \mathcal{L}}{\partial \mathbf{Z}}$ obtained by sampling $b-1$ rows uniformly at random without replacement, where each element of $\frac{\partial \mathcal{L}}{\partial \mathbf{Z}}$ is distributed i.i.d. as $\frac{\partial \mathcal{L}}{\partial \mathbf{Z}_{j,k}} = \zeta |\epsilon|$ with $\epsilon \sim \mathcal{N}(\mu = 0, \sigma^2 > 0)$ and $\zeta \sim \text{Bernoulli}(p = \frac{1}{2})$. We then have the probability q of \mathbf{A} having exactly one all-zero column and being full rank lower bounded by:*

$$\begin{aligned} q &\geq \frac{b}{2^{b-1}} \left(1 - \left(\frac{1}{2} + o_{b-1}(1)\right)^{b-1}\right) \\ &\geq \frac{b}{2^{b-1}} (1 - 0.939^{b-1}). \end{aligned}$$

Proof. We have the probability of one of the b columns being all zero as $\frac{b}{2^{b-1}}$ if the network has full rank, all other columns will not be all-zero.

Further, we have the probability of the submatrix $\mathbb{1}_{A_{>0}}$ being full rank conditioned on column i being all-zero as the probability of the matrix described by remaining $b - 1$ columns being non-singular. This probability is $1 - (\frac{1}{2} + o_{b-1}(1))^{b-1}$ (Tikhomirov, 2020) where $\lim_{b \rightarrow \infty} o_{b-1}(1) = 0$, which can be lower-bounded with $1 - 0.939^{b-1}$ (Tao & Vu, 2005). We thus obtain their joint probability as their product. \square

Lemma 5.2. *Assuming i.i.d. submatrices \mathbf{A} following the distribution outlined in Lemma 5.1 and using Algorithm 1, we have the expected number of submatrices n_{total}^* required to recover all b correct direction vectors as:*

$$n_{total}^* = \frac{1}{q} \sum_{k=0}^{b-1} \frac{b}{b-k} = \frac{bH_b}{q} \approx \frac{1}{q} (b \log(b) + \gamma b + \frac{1}{2}),$$

where H_b is the b^{th} harmonic number and $\gamma \approx 0.57722$ the Euler-Mascheroni constant.

Proof. As we sample submatrices \mathbf{A} uniformly at random with replacement, assuming them to be i.i.d. is well justified for the regime of $m \gg b$. The number n of submatrices drawn between correct direction vectors \mathbf{q}_i thus follows a Geometric distribution $\mathbb{P}[n = k] = q(1 - q)^{k-1}$ with success probability q with expectation $n^* = \mathbb{E}[n] = \frac{1}{q}$. As we draw correct direction vectors \mathbf{q}_i uniformly at random from the b columns of $\overline{\mathbf{Q}}$, we have the probability of drawing a new direction vector \mathbf{q}_i as $\frac{b-k}{b}$ for k already drawn direction vectors. Again via the expectation of the Geometric distribution we obtain the expected number c^* of correct direction vectors we have to draw until we have recovered all b distinct ones as the solution of the Coupon Collector Problem $c^* = \sum_{k=0}^{b-1} \frac{b}{b-k} = bH_b \approx b \log(b) + \gamma b + \frac{1}{2}$. The proof concludes with the linearity of expectation. \square

Maximum Number of Samples Required with High Probability We now compute the number of samples n_{total}^p required to recover all b correct directions with high probability $1 - p$.

Lemma A.1. *In the same setting as Lemma 5.2, we have an upper bound n_{total}^p on the number of submatrices we need to sample until we have recovered all b correct direction vectors by solving the following quadratic inequality for n_{total}^p*

$$\frac{p}{2} \leq \Phi \left(\frac{b \log(2b/p^*) - n_{total}^p q}{\sqrt{n_{total}^p q(1-q)}} \right),$$

where Φ is the cumulative distribution function of the standard normal distribution and $p^* = p - 1 + (1 - p_{fr})^b$.

Proof. At a high level, bound the number of valid directions c^p we need to discover until we recover all b distinct ones and then the number of submatrices n_{total}^p we need to sample to obtain these c^p directions, each with probability $1 - \frac{p}{2}$, before applying the union bound.

However, we first note that with probability $1 - (1 - p_{fr})^b$ we will (repeatedly) reject a correct direction due to a lack of induced sparsity and thus fail irrespective of the number of samples we draw. We thus correct our failure probability budget from p to $p^* = p - 1 + (1 - p_{fr})^b$, using the union bound.

We now show how to compute the upper bound on the number of correct directions c^p we need to find until we have found all b distinct directions. To this end, we bound the probability of not sampling the i^{th} direction $\overline{\mathbf{q}}_i$ after finding c candidates as $p_{-i} = (1 - \frac{1}{b})^c \leq e^{-\frac{c}{b}}$. We can then bound the probability of missing any of the b directions using the union bound as $p_{-all} \leq \sum_{i=1}^b p_{-i} = be^{-\frac{c^p}{b}}$. We thus obtain the minimum number c^p of correct directions to find all b distinct ones with probability at least $\frac{p^*}{2}$ as $c^p \geq b \log(2b/p^*)$.

We can now compute the number n_{total}^p of samples required to find c^p submatrices satisfying the condition of Theorem 3.4 for some i with probability $1 - \frac{p}{2}$. To this end, we approximate the Binomial distribution $\mathcal{B}(n, q)$ with the normal distribution $\mathcal{N}(nq, nq(1-q))$ (Parameswaran, 1979), which is generally precise if $\min(nq, n(1-q)) > 9$ (Chen, 2011), which holds for $b \geq 5$. We thus obtain the number of samples n_{total}^p required to find r valid directions with high probability $1 - \frac{p^*}{2}$ by solving $\frac{p^*}{2} = \Phi \left(\frac{c^p - n_{total}^p q}{\sqrt{n_{total}^p q(1-q)}} \right)$ for n_{total}^p which boils down to a quadratic equation.

By the union bound, we have that the total failure probability of not finding all b correct directions is at most p . \square

For a batch size of $b = 10$ and $p = 10^{-8}$, we, e.g., obtain $n \approx 4 \times 10^4$.

Lemma 5.3. *Under the same assumptions as in Lemma 5.1, we have an upper bound on the failure probability p_{fail}^{ub} of Algorithm 1 even when sampling exhaustively as:*

$$p_{\text{fail}}^{ub} \leq b \left(1 - \sum_{k=b-1}^m \binom{m}{k} \frac{1}{2^m} \left(1 - 0.939^{(b-1)\binom{k}{b-1}} \right) \right) + 1 - (1 - p_{fr})^b,$$

where p_{fr} is the probability of a correct direction vector being falsely rejected by our sparsity filter (§4.1).

Proof. We will first compute the probability of $\frac{\partial \mathcal{L}}{\partial \mathbf{Z}}$ not containing a submatrix \mathbf{A} satisfying the conditions of Theorem 3.4 for all $i \in \{1, \dots, b\}$ and then the probability of us failing to discover it despite exhaustive sampling.

We observe that the number k of rows in $\frac{\partial \mathcal{L}}{\partial \mathbf{Z}}$ with a zero i^{th} entry is binomially distributed with success probability $\frac{1}{2}$. For each $k \geq b - 1$, we can construct $\binom{k}{b-1}$ submatrices \mathbf{A} with an all-zero i^{th} column. The probability of any such submatrix having full rank is $1 - (\frac{1}{2} - o_{b-1}(1))^{b-1} > 1 - 0.939^{b-1}$ (Tikhomirov, 2020; Tao & Vu, 2005).

We thus have the probability of $\frac{\partial \mathcal{L}}{\partial \mathbf{Z}}$ containing at least one submatrix \mathbf{A} with full rank and an all-zero i^{th} column as $\sum_{k=b-1}^m \binom{m}{k} \frac{1}{2^m} \left(1 - 0.939^{(b-1)\binom{k}{b-1}} \right)$.

Using the union bound, we thus obtain an upper bound on the probability of $\frac{\partial \mathcal{L}}{\partial \mathbf{Z}}$ not containing any submatrix \mathbf{A} with full rank and an all-zero i^{th} column for all $i \in \{1, \dots, b\}$.

To compute the probability of us failing to discover an existing submatrix despite exhaustive sampling, we first note that we have the probability p_{fr} of an arbitrary column in $\frac{\partial \mathcal{L}}{\partial \mathbf{Z}}$ being less sparse than our threshold τ . Thus, with probability $1 - (1 - p_{fr})^b$ we will discard at least one correct direction due to it inducing an unusually dense column in $\frac{\partial \mathcal{L}}{\partial \mathbf{Z}}$.

We now obtain the overall failure probability via the union bound. □

B. Deferred Algorithms

Here, we present the Algorithms COMPUTESIGMA and GREEDYFILTER referenced in §5.1.

Algorithm 2 COMPUTESIGMA

- 1: **INPUT:** $L, R, W, b, \frac{\partial \mathcal{L}}{\partial \mathbf{b}}, \mathcal{B}$
 - 2: $\mathbf{Q} \leftarrow \text{FIXSCALE}(\mathcal{B}, L, \frac{\partial \mathcal{L}}{\partial \mathbf{b}})$
 - 3: $\frac{\partial \mathcal{L}}{\partial \mathbf{Z}} \leftarrow L \cdot \mathbf{Q}$
 - 4: $\mathbf{X}^T \leftarrow \mathbf{Q}^{-1} \cdot R$
 - 5: $\mathbf{Z} = W \cdot \mathbf{X} + (\mathbf{b} | \dots | \mathbf{b})$
 - 6: $\sigma_- \leftarrow \sum_{i,j} \mathbb{1}[\mathbf{Z}_{i,j} \leq 0] \cdot \mathbb{1}[\frac{\partial \mathcal{L}}{\partial \mathbf{Z}_{i,j}} = 0]$
 - 7: $\sigma_+ \leftarrow \sum_{i,j} \mathbb{1}[\mathbf{Z}_{i,j} > 0] \cdot \mathbb{1}[\frac{\partial \mathcal{L}}{\partial \mathbf{Z}_{i,j}} \neq 0]$
 - 8: $\sigma \leftarrow \frac{\sigma_- + \sigma_+}{m \cdot b}$
 - 9: **return** σ
-

C. Dataset Licenses

In this work, we use the commonly used MNIST (LeCun et al., 2010), CIFAR-10 (Krizhevsky et al., 2009) and Tiny-ImageNet (Le & Yang, 2015) datasets. No information regarding licensing has been provided on their respective websites.

Algorithm 3 GREEDYFILTER

```

1: INPUT:  $L, R, W, b, \frac{\partial \mathcal{L}}{\partial b}, \mathcal{C}$ 
2:  $\mathcal{B} \leftarrow \{\}$ 
3: repeat
4:   Select the sparsest vector  $\bar{q}'_i$  from  $\mathcal{C} \setminus \mathcal{B}$ 
5:    $\mathcal{B} \leftarrow \mathcal{B} \cup \{\bar{q}'_i\}$ 
6:   if  $\mathcal{B}$  is not of full rank then
7:      $\mathcal{B} \leftarrow \mathcal{B} \setminus \{\bar{q}'_i\}$ 
8:   until rank of  $\mathcal{B}$  is  $B$ 
9:
10:  $\sigma \leftarrow \text{COMPUTESIGMA}(L, R, W, b, \frac{\partial \mathcal{L}}{\partial b}, \mathcal{B})$ 
11: repeat
12:   changed  $\leftarrow$  False
13:   for  $(\bar{q}'_i, \bar{q}'_j)$  in  $\mathcal{B} \times (\mathcal{C} \setminus \mathcal{B})$  do
14:      $\mathcal{B}' \leftarrow \mathcal{B} \setminus \{\bar{q}'_i\} \cup \{\bar{q}'_j\}$ 
15:      $\sigma' \leftarrow \text{COMPUTESIGMA}(L, R, W, b, \frac{\partial \mathcal{L}}{\partial b}, \mathcal{B}')$ 
16:     if  $\sigma' > \sigma$  then
17:        $\mathcal{B} \leftarrow \mathcal{B}'$ 
18:        $\sigma \leftarrow \sigma'$ 
19:     changed  $\leftarrow$  True
20: until not changed
21:  $Q \leftarrow \text{FIXSCALE}(\mathcal{B}, L, \frac{\partial \mathcal{L}}{\partial b})$ 
22:  $X^T \leftarrow Q^{-1} \cdot R$ 
23: return  $\sigma, X$ 

```

D. Deferred Experiments

D.1. Experiments on Label-Heterogeneous Data

In this section, we provide additional experiments on clients with heterogeneous data. In particular, we look at the extreme case where each client has data only from a single class. As label repetition makes optimization-based attacks harder (Geiping et al., 2020; Yin et al., 2021; Geng et al., 2021), the results presented in Table 2 for the TinyImageNet dataset demonstrate another advantage of our algorithm, namely, SPEAR works regardless of the label distribution, providing even better reconstruction results compared to Table 1 for single-label batches.

Table 2. Mean reconstruction quality metrics across 100 batches for batches only containing samples from one class.

Dataset	PSNR \uparrow	SSIM \uparrow	MSE \downarrow	LPIPS \downarrow	Acc. \uparrow
TINYIMGNET	127.7	0.999717	4.80×10^{-6}	10.36×10^{-5}	98%

D.2. Additional Experiments on Effect of Training on SPEAR

In Figure 7 in the main paper, we provided the results of evaluating SPEAR on a network in training on the same train data used for training. Here, we instead look at what happens if we evaluate the same network in training on fresh data coming from the MNIST test set. The results are presented in Figure 9. We observe similar trends, suggesting that our attack will work equally well on federated clients that already participated in the training, as on those that participate for the first time in later epochs.

D.3. Additional Experiments on Failure Probabilities

In this section, we provide more experiments validating our theoretical analysis of SPEAR’s failure rate for several additional batch sizes b . We present our results in Figure 10, where we observe similar trends to Figure 8, reaffirming our original results.

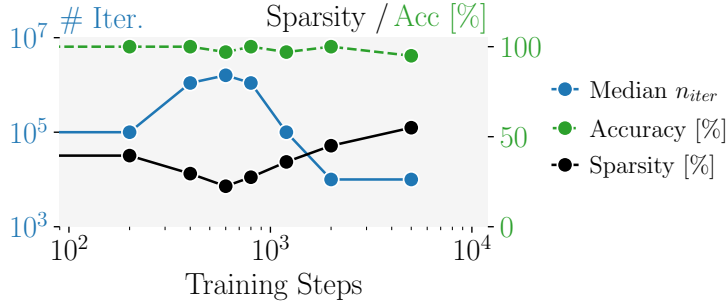


Figure 9. Effect of training on the effectiveness of SPEAR for batches from MNIST’s test set depending on the minimum column sparsity of $\frac{\partial \mathcal{L}}{\partial \mathbf{Z}}$ at a batch size of $b = 10$.

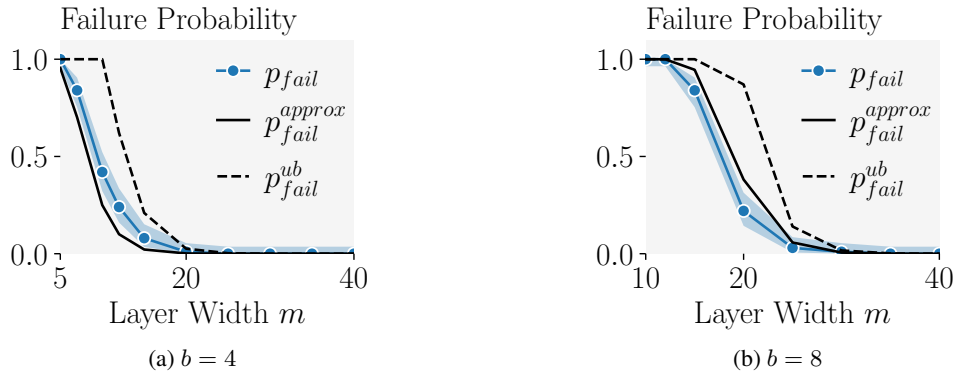


Figure 10. Empirical failure probability (blue) with 95% Clopper-Pearson confidence bounds (shaded blue) compared to the analytical upper bound (dashed line) and approximation (solid line) of the failure probability for further batch sizes b .

E. Visualisations of our results

Here we present a visual comparison between all batch images recovered by our method and Geiping et al. (2020) on TinyImageNet for a 6 layer fully connected network with width $m = 200$. In Figure 11 we operate in the same setting as App. D.1, namely batches of a single class. We observe that while some images are well reconstructed by Geiping et al. (2020), most of the images are of poor visual quality, with some even being hard to recognize. In contrast, all of our recovered images are pixel perfect. This in particular also means, that SPEAR’s reconstructions improve in fine-detail recovery even upon the well recovered images of Geiping et al. (2020). This is expected as our attack is exact (up numerical errors).

Finally, we demonstrate what happens to our proposed reconstructions in the rare cases when our algorithm fails to recover a batch, i.e., it fails to find or select some of the correct directions \bar{q}_i . In Figure 12, we show the one-and-only such batch for the experiment on TinyImageNet presented in Table 1. The batch had 2 wrong \bar{q}_i s and still achieves an average PSNR of 91.2, which is much higher compared to prior work. Further, all but 2 images are affected by the failure.

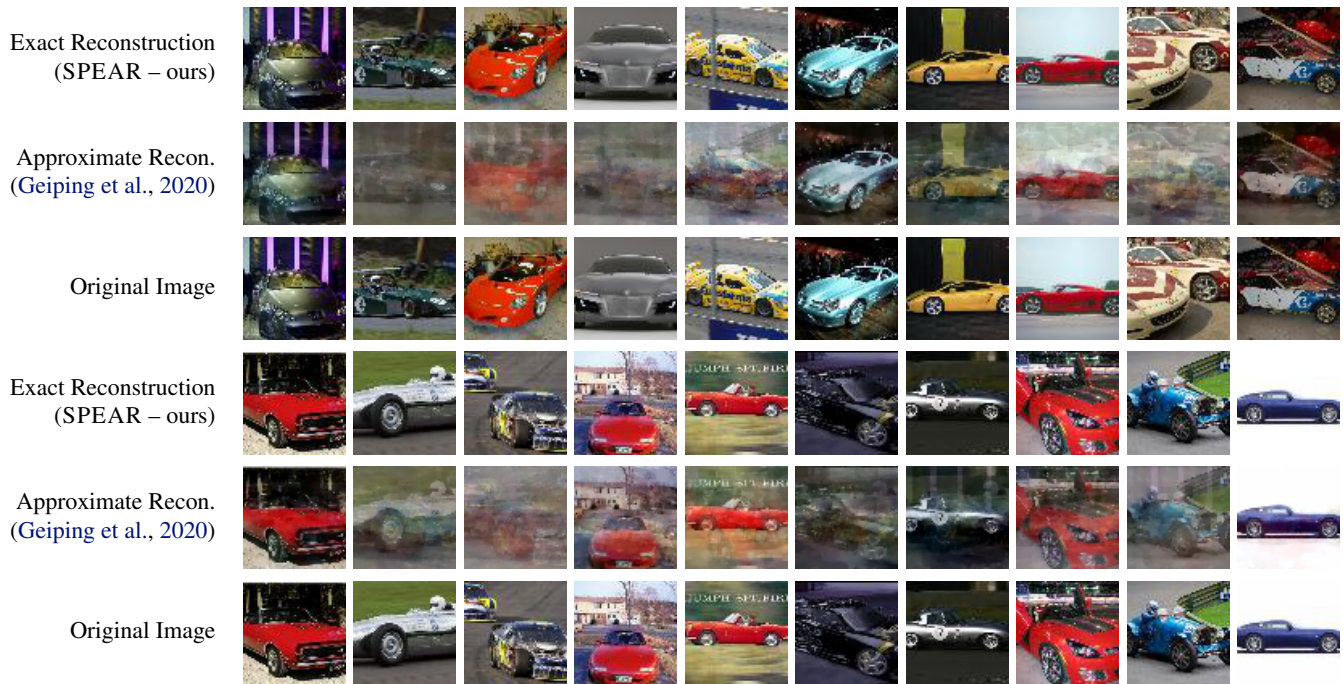


Figure 11. The reconstructions of all images from Figure 1, reconstructed using our SPEAR (top) or the prior state-of-the-art Geiping et al. (2020) (mid), compared to the ground truth (bottom).

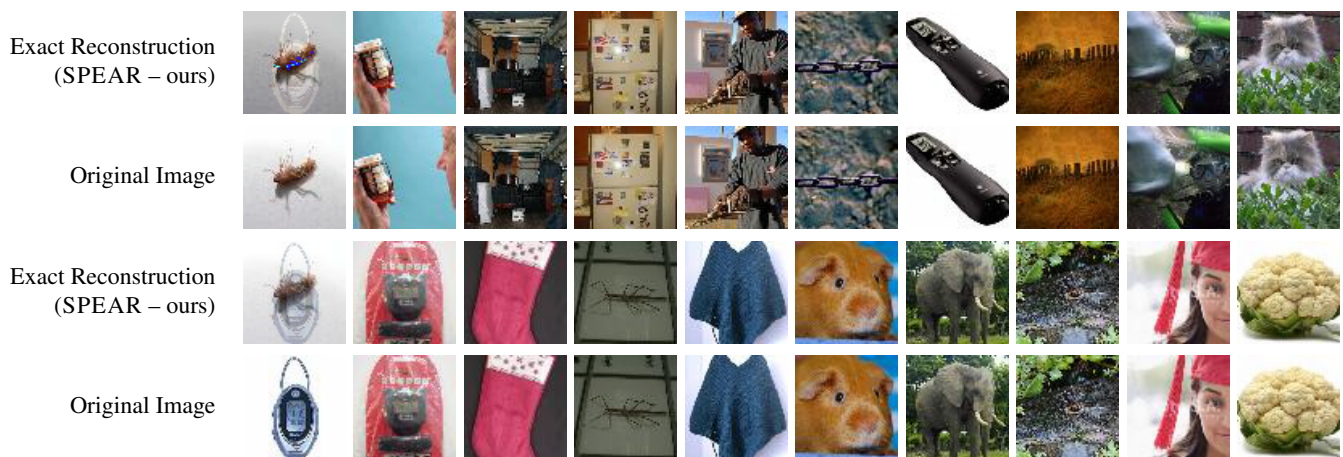


Figure 12. The only batch not perfectly reconstructed by SPEAR for the TinyImageNet experiment in Table 1. The reconstruction selected 2/20 wrong directions \hat{q}_i , resulting in the left most images being wrongly recovered.